DE GRUYTER DOI 10.1515/htmp-2013-0057 — High Temp. Mater. Proc. 2014; 33(4): 319–323

Jun-Hao Liu, Guo-Hua Zhang and Kuo-Chih Chou*

Reaction Kinetics of Fe_2O_3 and $BaCO_3$ to Prepare $Ba_2Fe_2O_5$

Abstract: Carbon dioxide is a greenhouse gas and substantially affects the global warming and climate change, so study on the adsorption of carbon dioxide is very urgent. As a new CO_2 captor, $Ba_2Fe_2O_5$ was prepared by the solid state reaction of Fe_2O_3 with $BaCO_3$, following formula $Fe_2O_3 + 2BaCO_3 = Ba_2Fe_2O_5 + 2CO_2$. The reaction kinetics in isothermal condition was investigated by using the method of thermo-gravimetric analyzer (TGA). It was found that the reaction of Fe_2O_3 with $BaCO_3$ was controlled by the diffusion step in the product layer, and the kinetics process could be described by the RPP model (Real Physical Picture) with the apparent activation energy extracted to be 161.122 kJ/mol.

Keywords: $Ba_2Fe_2O_5$, thermo-gravimetric analyzer, kinetics

---

***Corresponding author: Kuo-Chih Chou:** State Key Laboratory of Advanced Metallurgy, University of Science and Technology Beijing, Beijing 100083, China. E-mail: kcc126@126.com
Jun-Hao Liu, Guo-Hua Zhang: State Key Laboratory of Advanced Metallurgy, University of Science and Technology Beijing, Beijing 100083, China

1 Introduction

In recent years, the global warming phenomenon caused by greenhouse gases has become a serious environmental issue of common concern in the world, which causes more and more attention of governments [1–4]. Carbon dioxide from fossil fuel combustion is the main cause of the global warming. So it is a very important and urgent problem to find effective materials to capture and store CO_2. Up to now, several materials have been studied as CO_2 captors, for instance, zeolites, metal oxides, carbon-based materials, lithium-based ceramic, and so on [5–8]. In many cases, CO_2 emissions are favored by conditions of high temperature (power plant, iron making process, etc), meanwhile, the absorption rate of CO_2 at high temperature is much faster, so it is significant to find CO_2 captors which can be used at high temperature.

Li_2ZrO_3 was the first reported lithium-based ceramic for trapping CO_2, which absorbed CO_2 as follows,

$$Li_2ZrO_3(s) + CO_2(g) = Li_2CO_3(s) + ZrO_2(s) \quad (1)$$

The suitable adsorption temperature of this material is around 823–973 K and the desorption process takes place at above 973 K.

Li_4SiO_4 is another lithium-based CO_2 captor. Compared with Li_2ZrO_3, Li_4SiO_4 has a higher absorption and desorption rate [9]. CO_2 adsorption of Li_4SiO_4 is described by the following reaction:

$$Li_4SiO_4(s) + CO_2(g) = Li_2CO_3(s) + Li_2SiO_3(s) \quad (2)$$

In the standard condition, CO_2 adsorption reaction takes place below 973 K, while when the temperature exceeds 973 K the reaction proceeds toward the left side [10, 11].

Fujishiro et al. [12] found another CO_2 captor $Ba_2Fe_2O_5$ which showed desirable properties. The reaction of $Ba_2Fe_2O_5$ and CO_2 is shown below:

$$Ba_2Fe_2O_5(s) + CO_2(g) = BaCO_3(s) + BaFe_2O_4(s) \quad (3)$$

$Ba_2Fe_2O_5$ which has a higher adsorption temperature than the other CO_2 captors can absorb CO_2 in a wide temperature range of 773 K to 1373 K. When the temperature exceeds 1373 K, the desorption reaction of CO_2 takes place. So, it can be used as a good CO_2 captor for its high adsorption-desorption transition temperature. Generally, Fe_2O_3 and $BaCO_3$ were used as the raw materials to prepare $Ba_2Fe_2O_5$. However, there has been no detailed study on the reaction kinetics of Fe_2O_3 and $BaCO_3$ which is very important for the preparation of $Ba_2Fe_2O_5$, but it has great significance for preparing $Ba_2Fe_2O_5$, so it is an urgent task to study reaction kinetics. Consequently, it is the objective of the present paper to investigate the preparation kinetics of $Ba_2Fe_2O_5$ using Fe_2O_3 and $BaCO_3$ as raw materials.

2 Experimental procedure

$Ba_2Fe_2O_5$ was synthesized by solid-state reaction method, using barium carbonate ($BaCO_3$, analytically pure) and ferric sesquioxide (Fe_2O_3, analytically pure). Initially,

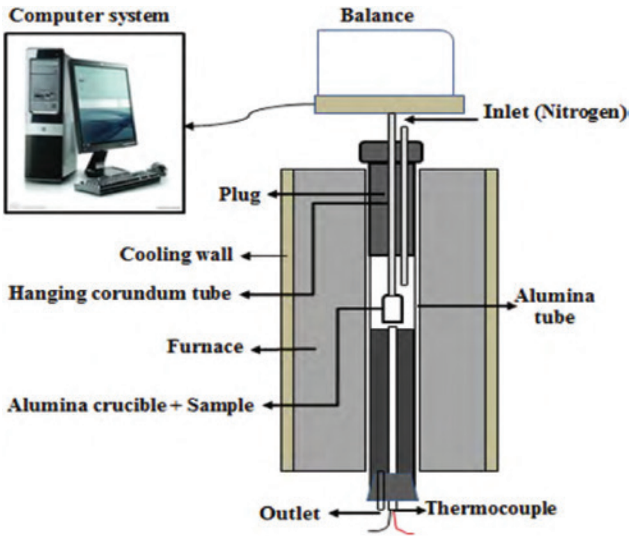

Fig. 1: Schematic diagram of the apparatus.

$BaCO_3$ and Fe_2O_3 powers were calcined at 423 K (423 K = 150 °C) for 10 h to remove the adsorbed water, and then they were weighed in the stoichiometric ratio of $Ba_2Fe_2O_5$ and mixed with ethanol in an alumina mortar. The mixture was pressed into a thin disk of 18 mm diameter at 0.4 Gpa. Then, the disks were calcined at 1273 K, 1373 K and 1473 K in N_2 gas flow to study the reaction kinetics of $BaCO_3$ and Fe_2O_3, in which process, the thermogravimetric analyzer was used to monitor the weight change of the disks which was continuously recorded with sensitivity of 0.001 g. Figure 1 shows the schematic diagram of the apparatus.

The obtained products at different temperatures were examined by XRD (Model, TTR III, Japan) to confirm whether the product was single phase $Ba_2Fe_2O_5$ or not. The morphologies of these products were observed by using SEM (Model S250MK3, CAMBRIDGE) technique.

3 Results and discussion

3.1 Effect of temperature

The isothermal reactions of $BaCO_3$ with Fe_2O_3 to prepare $Ba_2Fe_2O_5$ were conducted at the temperatures of 1273 K, 1373 K and 1473 K. The reacted fraction was calculated by using Eq. (4),

$$R = \frac{\Delta m_t}{\Delta m} \tag{4}$$

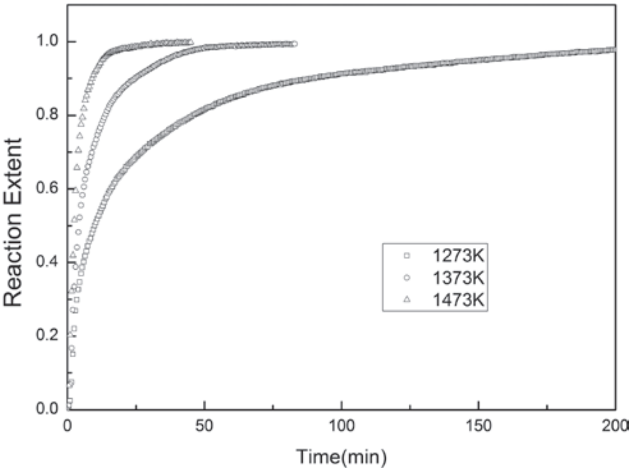

Fig. 2: The reacted fractions at different temperatures

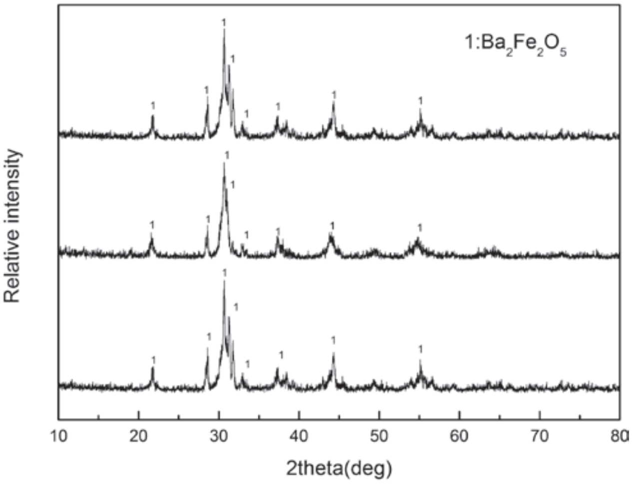

Fig. 3: The XRD patterns of reaction products at 1273 K, 1373 K and 1473 K

where Δm_t is the weight loss after time t; Δm is the theoretical maximum weight loss of the sample. The kinetics curves at different temperatures are shown in Figure 2, from which it can be concluded that the reaction rate increases quickly with increasing temperature. After reacting for 20 min, the increment of the dimensionless mass change was found to be much slower.

3.2 Reaction product analyzed by XRD

The XRD results of products are presented in Figure 3, from which it can be seen that the pure $Ba_2Fe_2O_5$ can be prepared by $BaCO_3$ and Fe_2O_3 in the temperature range of 1373 K to 1473 K. But the pattern sintered at 1273 K seems a little different from those sintered at other temperatures. It probably results from the fact that the crystallinity of the sample sintered at 1373 K and 1473 K is higher than that sintered at 1273 K.

3.3 SEM analysis

Figure 4(a) to (c) show the microstructures of products ($Ba_2Fe_2O_5$) prepared at 1273 K, 1373 K and 1473 K, respectively. From the SEM photographs of the $Ba_2Fe_2O_5$, it is found that the particle sizes of the samples sintered at the higher temperature are larger than that of the samples sintered at the lower temperature. The reason for this phenomenon may be that the higher the temperature, the higher the rate of grain growth will be.

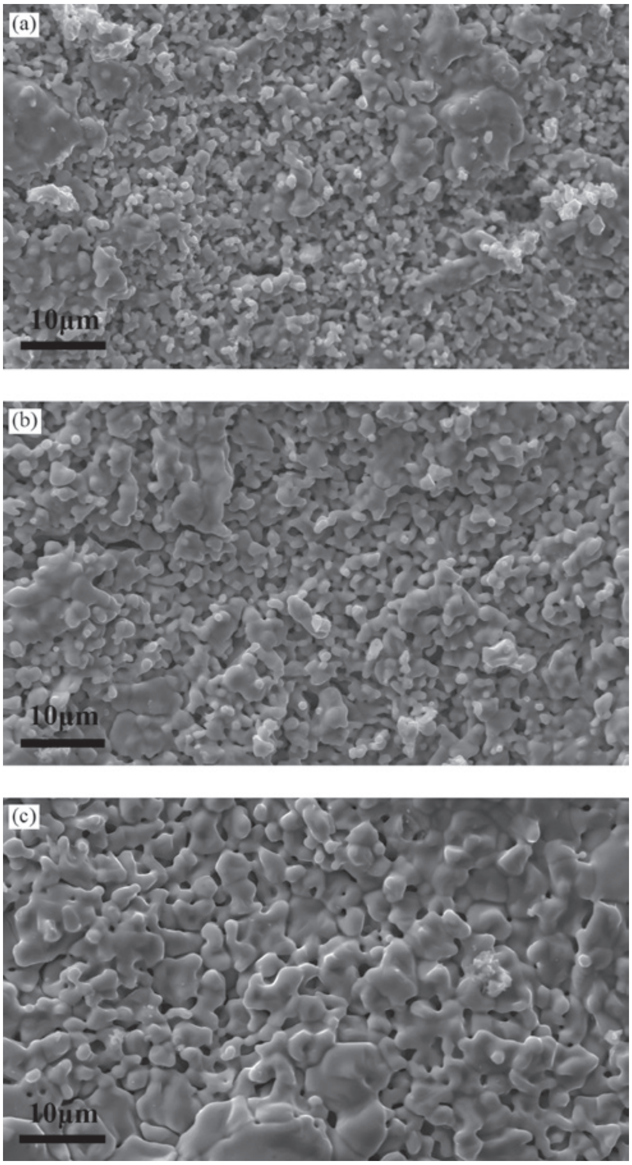

Fig. 4: SEM photos of products ($Ba_2Fe_2O_5$) at (a) 1273 K, (b) 1373 K, and (c) 1473 K

3.4 Reaction kinetics

The reaction between Fe_2O_3 and $BaCO_3$ proceeds first at the outer surface to form a thin $Ba_2Fe_2O_5$ product layer. As the reaction continues, the product becomes thicker and thicker, and the resistance from the solid product layer become larger and larger. Therefore, the rate of the whole reaction will be controlled by the diffusion in the product layer.

Chou et al. [13–15] have proposed a RPP (Real Physical Picture) model to describe the kinetics of reaction controlled by the diffusion process in the solid-product layer, as shown in Eqs. (5) and (6). The RPP model is analytic with a form of explicit function; therefore, it is not only easy to use but also enables the easy performance of a theoretical analysis. Next, the RPP model will be used to describe the reaction kinetics of $BaCO_3$ and Fe_2O_3.

$$\xi = 1 - (1 - \sqrt{\frac{\exp(-\Delta E / RT)t}{B_T}})^3 \tag{5}$$

where

$$B_T = \frac{1}{(2K_o^{o\beta} D_o^{o\beta} / v_m)((\sqrt{P_{CO_2}} - \sqrt{P_{CO_2}^{eq}}) / R_o^2)} \tag{6}$$

where ΔE represents the apparent activation energy; B_T is a function of P_{CO_2}, $P_{CO_2}^{eq}$ and R_o, in which $P_{CO_2}^{eq}$ is the carbon dioxide partial pressure in equilibrium with oxide and should be related to the temperature; $K_o^{o\beta}$ and $D_o^{o\beta}$ are constant independent of temperature; v_m is a coefficient that depends on substance and reaction; R_0 is the radius of the particle. If the value of $P_{CO_2}^{eq}$ is very small or the temperature coefficient of $P_{CO_2}^{eq}$ can be neglected, B_T will be constant as the carbon dioxide partial pressure and the particle radius are fixed.

3.5 Application of the new model

Eq. (5) can be used to describe the reaction kinetics of Fe_2O_3 and $BaCO_3$ in isothermal conditions. The fitting results are shown in Figure 5, from which it can be seen that the experimental data and theoretical predicted

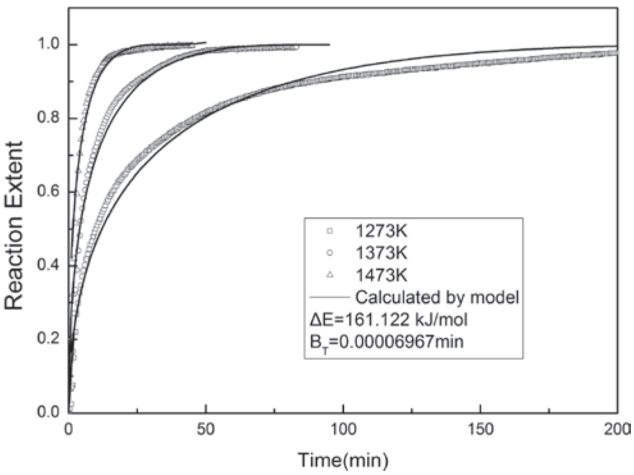

Fig. 5: A comparison between experimental data and theoretical predictions from the RPP model at different temperatures

values are in good agreement validating the present theoretical approach. The apparent activation energy and parameter B_T can be extracted to be 161.122 kJ/mol and 0.00006967 min, respectively. The model describing the effects of temperature and time on the reacted fraction is given as follows:

$$\xi = 1-[1-\sqrt{\frac{\exp(-161122.05/RT)t}{0.00006967}}]^3 \qquad (7)$$

3.6 Comparison with Jander model

Jander [16] proposed a diffusion-controlled coreshell model to correlate the reacted fraction with time. The integral form of Jander equation is

$$\xi = 1-(1-\sqrt{kt})^3 \qquad (8)$$

where k is the rate constant which depends on temperature, radius of particle and partial pressure, etc. The temperature of k can be described by the Arrhenius equation, $k = A\exp(-\Delta E/RT)$, where A is the pre-exponential factor, ΔE is the activation energy. The physical meaning of k in Eq. (8) is not as clear as the parameters in Eq. (5). When using the Jander equation, it is commonly to regress the rate constants at different temperatures by Eq. (8) first, and then extract activation energy by Arrhenius equation with the values of rate constants.

Figure 6 and Figure 7 show the fitting results of Jander model. Compared with Figure 5, it can be seen that the RPP model has more advantages than Jander model and can well describe the reaction kinetics of Fe_2O_3 and $BaCO_3$ to prepare $Ba_2Fe_2O_5$.

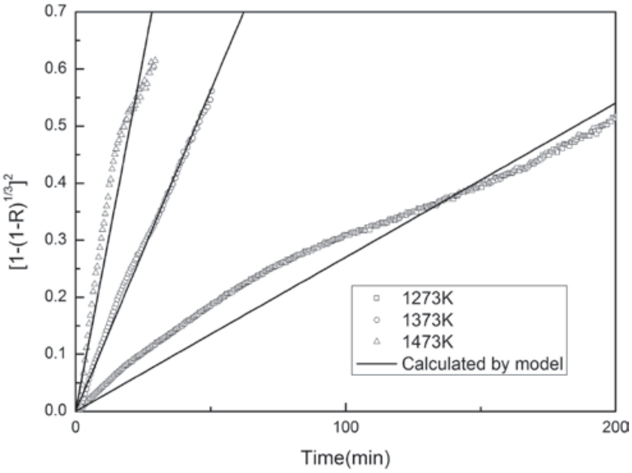

Fig. 6: Plots of $[1-(1-R)^{1/3}]^2$ vs. time for reaction of Fe_2O_3 and $BaCO_3$ at different temperatures

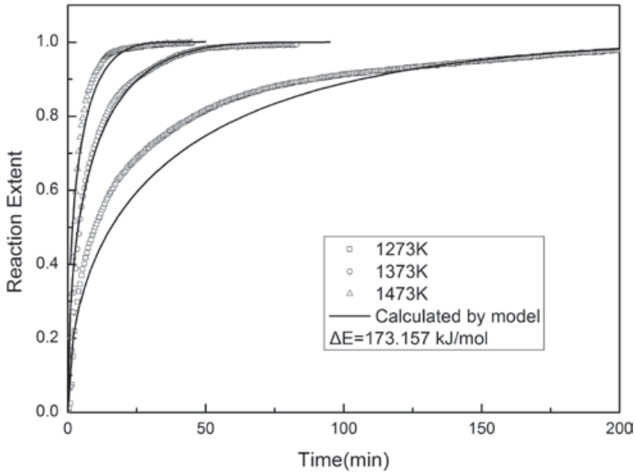

Fig. 7: A comparison between experimental data and theoretical predictions from Jander model at different temperatures

4 Conclusion

The reaction kinetics of preparing $Ba_2Fe_2O_5$ using Fe_2O_3 and $BaCO_3$ was investigated by TG measurement in the temperature range of 1273 K to 1473 K. From the comparison of measured kinetic curves with calculated results, it can be concluded that diffusion in the $Ba_2Fe_2O_5$ product is the rate-controlling step of the reaction of Fe_2O_3 with $BaCO_3$. The apparent activation energy calculated by the RPP model is extracted to be 161.122 kJ/mol.

Received: June 18, 2013. Accepted: September 10, 2013.

References

[1] M.S. Kwak, J.S. Hwang, C.O. Park, N. Miura and N. Yamazoe, *Sens. Actuators B*, **56**, 59–64 (1999).

[2] E.J. Karlsen, M.A. Nygren and G.M. Pettersson, *J. Phys. Chem. B*, **107**, 7795–7802 (2003).

[3] J.W. Dijkstra and D. Jansen, *Energy*, **29**, 1249–1257 (2004).

[4] X. Wei, X. Liu and M. Deeba, *Appl. Catal. B: EnViron*, **58**, 41–49 (2005).

[5] Z. Yong and A.E. Rodrigues, *Energy ConVers. Manage*, **43**, 1865–1876 (2002).

[6] S.K. Wirawan and D. Creaser, *Microporous Mesoporous Mater*, **91**, 196–205 (2006).

[7] A. Macario, A. Katovic, G. Giordano, F. Iucolano and D. Caputo, *Microporous Mesoporous Mater*, **81**, 139–147 (2005).

[8] K. Nomura, K. Tokumistu, T. Hayakawa and Z. Homonnay, *J. Radioanal. Nucl. Chem.*, **246**, 69–77 (2000).

[9] R. Xiong, J. Ida and Y.S. Lin, *Chem. Eng. Sci.*, **58**, 4377–4385 (2003).

[10] I. Junichi and Y.S. Lin, *J. Environ. Sci. Technol.*, **37**, 1999–2004 (2003).

[11] I. Junichi and Y.S. Lin, *Separation and Purification Technology*, **36**, 41–51 (2004).

[12] F. Fujishiro, K. Fukasawa, and T. Hashimoto, *J. Am. Ceram. Soc.*, **94**, 3675–3678 (2011).

[13] K.C. Chou, Q. Li, L. Lin, J. Jiang and K.D. Xu, *Int. J. Hydrogen Energ.*, **30**, 301–309 (2005).

[14] K.C. Chou and X.M. Hou, *J. Am. Ceram. Soc.*, **92**, 585–594 (2009).

[15] K.C. Chou, *J. Am. Ceram. Soc.*, **89**, 1568–1576 (2006).

[16] W. Jander, *Z. Anorg. Allg. Chem.*, **163**, 1–30 (1927).